

## S and P-wave heavy-light mesons in lattice NRQCD

Randy Lewis

*Department of Physics, University of Regina, Regina, SK, Canada S4S 0A2*

R. M. Woloshyn

*TRIUMF, 4004 Wesbrook Mall, Vancouver, BC, Canada V6T 2A3*

(March 2000)

### Abstract

The mass spectrum of S and P-wave mesons containing a single heavy quark is computed in the quenched approximation, using NRQCD up to third order in the inverse heavy quark mass expansion. Previous results found third order contributions which are as large in magnitude as the total second order contribution for the charmed S-wave spin splitting. The present work considers variations such as anisotropic lattices, Landau link tadpole improvement, and a highly-improved light quark action, and finds that the second order correction to the charmed S-wave spin splitting is about 20% of the leading order contribution, while the third order correction is about 20%(10%) for  $D^* - D(D_s^* - D_s)$ . Nonleading corrections are very small for the bottom meson spectrum, and are statistically insignificant for the P-wave charmed masses. The relative orderings among P-wave charmed and bottom mesons, and the sizes of the mass splittings, are discussed in light of experimental data and existing calculations.

## I. INTRODUCTION

Calculations in QCD can be performed numerically on a discrete space-time lattice, provided the lattice spacing is small enough to accommodate all of the relevant physical distance scales. In the presence of a heavy quark the lattice spacing must be small relative to the inverse quark mass, resulting in large computational requirements, unless an appropriate “effective theory” is used. In particular, for the case of a hadron containing exactly one heavy quark, the dynamics can be expanded in powers of the inverse heavy quark mass using the well-established technique of heavy quark effective theory [1] or nonrelativistic QCD (NRQCD) [2,3]. With the heavy quark expansion, the lattice spacing can be much coarser and the computational requirements are correspondingly smaller.

In the present work, two issues will be addressed within quenched lattice NRQCD. Firstly, is the charm quark sufficiently heavy to permit the use of lattice NRQCD for charmed meson spectroscopy? Secondly, what are the mass splittings (magnitude and sign) between P-wave mesons containing a single heavy quark?

The first issue is clearly of interest due to the computational efficiency of lattice NRQCD. The heavy quark expansion is known to work well for bottom mesons [4,5], but previous research has demonstrated that  $O(1/M^2)$  and  $O(1/M^3)$  contributions can be comparable in magnitude for the S-wave spin splitting of charmed mesons. [4] The present work provides an extension of this investigation by considering new simulations that incorporate a number of changes in method. For example, Ref. [4] used the fourth root of an elementary plaquette to define the tadpole improvement factor,  $U_0$ , whereas the present work uses the mean link in Landau gauge. Since the Landau definition is advantageous in other contexts [6], including the velocity expansion for the charmonium spectrum of lattice NRQCD [7], it might be expected to improve the convergence of the heavy quark expansion for the charmed heavy-light spectrum as well. Also, the light quark was described by the Sheikholeslami-Wohlert action in Ref. [4], but the present work uses a D234 action [8] which has smaller lattice spacing errors classically. The simulations in the present work differ from those of Ref. [4] in various other ways as well, including Dirichlet versus periodic boundary conditions for light quark propagation, differing discretizations for heavy quark propagation, and the introduction of an anisotropic lattice with a smaller temporal lattice spacing than spatial spacing. Despite these modifications, the present simulations produce a conclusion similar to that of Ref. [4]: the  $O(1/M^2)$  and  $O(1/M^3)$  contributions are comparable in magnitude for the S-wave charmed spin splitting; in the present work, each is roughly 20% of the  $O(1/M)$  result for  $D^* - D$ , though the  $O(1/M^3)$  contribution is closer to 10% for  $D_s^* - D_s$ .

The second issue under discussion relates to the spectrum of P-wave mesons containing a single heavy quark. The relative orderings of the P-wave bottom mesons have only recently come under direct experimental scrutiny [9–13], and the complete picture is not yet clear. Meanwhile theoretical predictions differ from one another even at a qualitative level. The traditional expectation of a hydrogen-like spectrum that arises from a number of model calculations [14–18] has been questioned long ago by Schnitzer [19] and very recently by Isgur [20] and by Ebert, Galkin and Faustov [21].

The calculation is difficult within lattice QCD because the P-wave splittings are not large in comparison to the typical scale of nonperturbative QCD, and because of operator mixing for the pair of P-wave states having  $J = 1$ . Some previous attempts have been made

[22–26]. Unfortunately, the uncertainties are often substantial, and results are not always as consistent with one another as might have been hoped. The present work represents a further comment on this situation. In particular, the  $D_{s2}^* - D_{s0}^*$  mass splitting is found to be positive as in the traditional hydrogen-like ordering, and to be substantially less than 100 MeV, while the  $D_2^* - D_0^*$ ,  $B_{s2}^* - B_{s0}^*$  and  $B_2^* - B_0^*$  splittings are even smaller. These splittings are consistent with a number of model calculations, but are somewhat smaller than the lattice NRQCD calculation of Ref. [25].

## II. ACTION

The lattice action has three terms: gauge action, light quark action and heavy quark action. The entire action is classically and tadpole-improved with the tadpole factors,  $u_s$  and  $u_t$ , defined as the mean links in Landau gauge in a spatial and temporal direction, respectively.

The gauge field action is

$$\begin{aligned}
S_G(U) = & \frac{5\beta}{3} \left[ \frac{1}{u_s^4 \xi} \sum_{\text{ps}} \left( 1 - \frac{1}{3} \text{ReTr} U_{\text{ps}} \right) - \frac{1}{20u_s^6 \xi} \sum_{\text{rs}} \left( 1 - \frac{1}{3} \text{ReTr} U_{\text{rs}} \right) \right. \\
& + \frac{\xi}{u_s^2 u_t^2} \sum_{\text{pt}} \left( 1 - \frac{1}{3} \text{ReTr} U_{\text{pt}} \right) - \frac{\xi}{20u_s^4 u_t^2} \sum_{\text{rst}} \left( 1 - \frac{1}{3} \text{ReTr} U_{\text{rst}} \right) \\
& \left. - \frac{\xi}{20u_s^2 u_t^4} \sum_{\text{rts}} \left( 1 - \frac{1}{3} \text{ReTr} U_{\text{rts}} \right) \right], \tag{1}
\end{aligned}$$

where  $\xi \equiv a_s/a_t$ . The subscripts “ps” and “rs” denote spatial plaquettes and spatial planar  $1 \times 2$  rectangles respectively. Plaquettes in the temporal-spatial planes are denoted by “pt”, while rectangles with the long side in a spatial(temporal) direction are labeled by “rst” (“rts”). The leading classical errors of this action are quartic in lattice spacing.

For light quarks, a D234 action [8] is used with parameters set to their tadpole-improved classical values. Its leading classical errors are cubic in lattice spacing.

$$\begin{aligned}
S_F(\bar{q}, q; U) = & \frac{4\kappa}{3} \sum_{x,i} \left[ \frac{1}{u_s \xi^2} D_{1i}(x) - \frac{1}{8u_s^2 \xi^2} D_{2i}(x) \right] + \frac{4\kappa}{3} \sum_x \left[ \frac{1}{u_t} D_{1t}(x) - \frac{1}{8u_t^2} D_{2t}(x) \right] \\
& + \frac{2\kappa}{3u_s^4 \xi^2} \sum_{x,i < j} \bar{\psi}(x) \sigma_{ij} F_{ij}(x) \psi(x) + \frac{2\kappa}{3u_s^2 u_t^2 \xi} \sum_{x,i} \bar{\psi}(x) \sigma_{0i} F_{0i}(x) \psi(x) \\
& - \sum_x \bar{\psi}(x) \psi(x), \tag{2}
\end{aligned}$$

where

$$D_{1i}(x) = \bar{\psi}(x) (1 - \xi \gamma_i) U_i(x) \psi(x + \hat{i}) + \bar{\psi}(x + \hat{i}) (1 + \xi \gamma_i) U_i^\dagger(x) \psi(x), \tag{3}$$

$$D_{1t}(x) = \bar{\psi}(x) (1 - \gamma_4) U_4(x) \psi(x + \hat{t}) + \bar{\psi}(x + \hat{t}) (1 + \gamma_4) U_4^\dagger(x) \psi(x), \tag{4}$$

$$\begin{aligned}
D_{2i}(x) = & \bar{\psi}(x) (1 - \xi \gamma_i) U_i(x) U_i(x + \hat{i}) \psi(x + 2\hat{i}) \\
& + \bar{\psi}(x + 2\hat{i}) (1 + \xi \gamma_i) U_i^\dagger(x + \hat{i}) U_i^\dagger(x) \psi(x), \tag{5}
\end{aligned}$$

$$D_{2t}(x) = \bar{\psi}(x)(1 - \gamma_4)U_4(x)U_4(x + \hat{t})\psi(x + 2\hat{t}) + \bar{\psi}(x + 2\hat{t})(1 + \gamma_4)U_4^\dagger(x + \hat{t})U_4^\dagger(x)\psi(x), \quad (6)$$

$$gF_{\mu\nu}(x) = \frac{1}{2i} \left( \Omega_{\mu\nu}(x) - \Omega_{\mu\nu}^\dagger(x) \right) - \frac{1}{3} \text{Im} \left( \text{Tr} \Omega_{\mu\nu}(x) \right), \quad (7)$$

$$\begin{aligned} \Omega_{\mu\nu} = & \frac{-1}{4} \left[ U_\mu(x)U_\nu(x + \hat{\mu})U_\mu^\dagger(x + \hat{\nu})U_\nu^\dagger(x) \right. \\ & + U_\nu(x)U_\mu^\dagger(x - \hat{\mu} + \hat{\nu})U_\nu^\dagger(x - \hat{\mu})U_\mu(x - \hat{\mu}) \\ & + U_\mu^\dagger(x - \hat{\mu})U_\nu^\dagger(x - \hat{\mu} - \hat{\nu})U_\mu(x - \hat{\mu} - \hat{\nu})U_\nu(x - \hat{\nu}) \\ & \left. + U_\nu^\dagger(x - \hat{\nu})U_\mu(x - \hat{\nu})U_\nu(x + \hat{\mu} - \hat{\nu})U_\mu^\dagger(x) \right]. \end{aligned} \quad (8)$$

The heavy quark action is NRQCD [2], which is discretized to give the following Green's function propagation:

$$G_{\tau+1} = \left( 1 - \frac{a_t H_B}{2} \right) \left( 1 - \frac{a_t H_A}{2n} \right)^n \frac{U_4^\dagger}{u_t} \left( 1 - \frac{a_t H_A}{2n} \right)^n \left( 1 - \frac{a_t H_B}{2} \right) G_\tau, \quad (9)$$

with  $n = 5$  chosen for this work. Separation of the Hamiltonian into two terms,  $H = H_A + H_B$ , is important for ensuring stability of the discretization. For example, recall the discussion in Ref. [4] of a large nonzero vacuum expectation value for the term containing  $c_{10}$  in the Hamiltonian (see Eq. (15)). This issue will be discussed further in Sec. IV.

The following Hamiltonian, written in terms of the bare heavy quark mass  $M$ , is complete to  $O(1/M^3)$  in the classical continuum limit [27]:

$$H = H_0 + \delta H, \quad (10)$$

$$H_0 = \frac{-\Delta^{(2)}}{2M}, \quad (11)$$

$$\delta H = \delta H^{(1)} + \delta H^{(2)} + \delta H^{(3)} + O(1/M^4) \quad (12)$$

$$\delta H^{(1)} = -\frac{c_4}{u_s^4} \frac{g}{2M} \boldsymbol{\sigma} \cdot \tilde{\mathbf{B}} + c_5 \frac{a_s^2 \Delta^{(4)}}{24M}, \quad (13)$$

$$\delta H^{(2)} = \frac{c_2}{u_s^2 u_t^2} \frac{ig}{8M^2} (\tilde{\Delta} \cdot \tilde{\mathbf{E}} - \tilde{\mathbf{E}} \cdot \tilde{\Delta}) - \frac{c_3}{u_s^2 u_t^2} \frac{g}{8M^2} \boldsymbol{\sigma} \cdot (\tilde{\Delta} \times \tilde{\mathbf{E}} - \tilde{\mathbf{E}} \times \tilde{\Delta}) - c_6 \frac{a_s (\Delta^{(2)})^2}{16n\xi M^2}, \quad (14)$$

$$\begin{aligned} \delta H^{(3)} = & -c_1 \frac{(\Delta^{(2)})^2}{8M^3} - \frac{c_7}{u_s^4} \frac{g}{8M^3} \left\{ \tilde{\Delta}^{(2)}, \boldsymbol{\sigma} \cdot \tilde{\mathbf{B}} \right\} - \frac{c_9 ig^2}{8M^3} \boldsymbol{\sigma} \cdot \left( \frac{\tilde{\mathbf{E}} \times \tilde{\mathbf{E}}}{u_s^4 u_t^4} + \frac{\tilde{\mathbf{B}} \times \tilde{\mathbf{B}}}{u_s^8} \right) \\ & - \frac{c_{10} g^2}{8M^3} \left( \frac{\tilde{\mathbf{E}}^2}{u_s^4 u_t^4} + \frac{\tilde{\mathbf{B}}^2}{u_s^8} \right) - c_{11} \frac{a_s^2 (\Delta^{(2)})^3}{192n^2 \xi^2 M^3}. \end{aligned} \quad (15)$$

The coefficients of the Hamiltonian are chosen so the dimensionless parameters,  $c_i$ , are unity at the classical level. As will be discussed below, computations have been performed with the  $c_i$  set to unity or zero in various combinations, including separate computations at  $O(1/M)$ ,  $O(1/M^2)$  and  $O(1/M^3)$  to allow discussions of convergence for the  $1/M$  expansion. Throughout this work,  $H_0$  is always placed in  $H_A$  of Eq. (9) and all of the remaining terms except the  $c_{10}$  term are only placed in  $H_B$ . The difference between having the  $c_{10}$  term in  $H_A$  or  $H_B$  will be discussed explicitly, since it has the nonzero vacuum expectation value.

A tilde on any quantity indicates that the leading discretization errors have been removed. In particular,

$$\tilde{E}_i = \tilde{F}_{4i}, \quad (16)$$

$$\tilde{B}_i = \frac{1}{2}\epsilon_{ijk}\tilde{F}_{jk}, \quad (17)$$

where [3]

$$\begin{aligned} \tilde{F}_{\mu\nu}(x) = & \frac{5}{6}F_{\mu\nu}(x) - \frac{1}{6u_\mu^2}U_\mu(x)F_{\mu\nu}(x + \hat{\mu})U_\mu^\dagger(x) - \frac{1}{6u_\mu^2}U_\mu^\dagger(x - \hat{\mu})F_{\mu\nu}(x - \hat{\mu})U_\mu(x - \hat{\mu}) \\ & - (\mu \leftrightarrow \nu). \end{aligned} \quad (18)$$

The various spatial lattice derivatives are defined as follows:

$$a_s\Delta_i G(x) = \frac{1}{2u_s}[U_i(x)G(x + \hat{i}) - U_i^\dagger(x - \hat{i})G(x - \hat{i})], \quad (19)$$

$$a_s\Delta_i^{(+)} G(x) = \frac{U_i(x)}{u_s}G(x + \hat{i}) - G(x), \quad (20)$$

$$a_s\Delta_i^{(-)} G(x) = G(x) - \frac{U_i^\dagger(x - \hat{i})}{u_s}G(x - \hat{i}), \quad (21)$$

$$a_s^2\Delta_i^{(2)} G(x) = \frac{U_i(x)}{u_s}G(x + \hat{i}) - 2G(x) + \frac{U_i^\dagger(x - \hat{i})}{u_s}G(x - \hat{i}), \quad (22)$$

$$\tilde{\Delta}_i = \Delta_i - \frac{a_s^2}{6}\Delta_i^{(+)}\Delta_i\Delta_i^{(-)}, \quad (23)$$

$$\Delta^{(2)} = \sum_i \Delta_i^{(2)}, \quad (24)$$

$$\tilde{\Delta}^{(2)} = \Delta^{(2)} - \frac{a_s^2}{12}\Delta^{(4)}, \quad (25)$$

$$\Delta^{(4)} = \sum_i \left(\Delta_i^{(2)}\right)^2. \quad (26)$$

This NRQCD action has quadratic classical lattice spacing errors.

### III. METHOD

The data presented here come from 2000 gauge field configurations on  $10^3 \times 30$  lattices at  $\beta = 2.1$  with a bare aspect ratio of  $\xi \equiv a_s/a_t = 2$ . Two light quark masses are used, corresponding to  $\kappa = 0.23$  and  $0.24$ . Fixed time boundaries are used for the light quark propagators so they fit naturally into a heavy-light meson, since the NRQCD heavy quark propagator is also not periodic in the temporal direction.

A calculation of the string tension from these gauge field configurations provides a determination of the renormalized anisotropy:

$$\xi \equiv a_s/a_t = 1.96(2). \quad (27)$$

TABLE I. Heavy-light meson creation operators.

$^{2S+1}L_J$	$\Omega(\vec{x})$
$^1S_0$	$(0, I)$
$^3S_1$	$(0, \sigma_i)$
$^1P_1$	$(0, \Delta_i)$
$^3P_0$	$(0, \sum_i \Delta_i \sigma_i)$
$^3P_1$	$(0, \Delta_i \sigma_j - \Delta_j \sigma_i)$
$^3P_2$	$(0, \Delta_i \sigma_i - \Delta_j \sigma_j)$ or $(0, \Delta_i \sigma_j + \Delta_j \sigma_i), i \neq j$

Using light quarks only, the lightest pseudoscalar and vector meson masses are easily obtained from local creation operators. By linear interpolation and extrapolation in  $1/\kappa$ , the critical ( $\kappa_c$ ) and strange ( $\kappa_s$ ) hopping parameters and the temporal lattice spacing are found to be

$$\kappa_c = 0.243025(41), \quad (28)$$

$$\kappa_s = \begin{cases} 0.2344(11) & \text{from } m_\phi, \\ 0.2356(3) & \text{from } m_K, \end{cases} \quad (29)$$

$$a_t = 0.1075(23)\text{fm from } m_\rho. \quad (30)$$

For the hopping parameters used in explicit computations,  $\kappa = 0.23$  and  $0.24$ , the ratio of pseudoscalar to vector meson masses is “ $m_\pi/m_\rho$ ” =  $0.815(3)$  and  $0.517(8)$  respectively. No exceptional configurations were encountered at these  $\kappa$  values. One might expect a systematic uncertainty on  $a_t$  to account for deviations from the linear relationship between  $a_t m_\rho$  and  $1/\kappa$ . The uncertainty is presumably a few percent, but cannot be estimated using only the two  $\kappa$  values studied here.

A heavy-light meson is created by the following operator,

$$\sum_{\vec{x}} Q^\dagger(\vec{x}) \Omega(\vec{x}) \Gamma(\vec{x}) q(\vec{x}), \quad (31)$$

where  $\Omega(\vec{x})$  is given in Table I and the smearing operator is

$$\Gamma(\vec{x}) = [1 + c_s \Delta^{(2)}(\vec{x})]^{n_s}. \quad (32)$$

All plots shown here use  $(c_s, n_s) = (0.15, 10)$  at the source and a local sink. The source is fixed at timestep 4, which is a distance  $3a_t$  from the lattice boundary.

Because NRQCD is an expansion in the inverse *bare* heavy quark mass, all meson mass differences can be obtained from correlation functions at  $\mathbf{p} = \mathbf{0}$ , but the absolute meson mass itself cannot be obtained directly. One way to determine the mass is to compute the change in energy when a meson is boosted,

$$E_{\mathbf{p}} - E_0 = \frac{\mathbf{p}^2}{2M_{\text{kin}}}. \quad (33)$$

This defines the kinetic mass,  $M_{\text{kin}}$ , which is interpreted as the meson’s physical mass. For the present work,  $E_{\mathbf{p}}$  is computed only for the  $^1S_0$  state, with  $\mathbf{p} = (0, 0, 2\pi/L_s)$  where

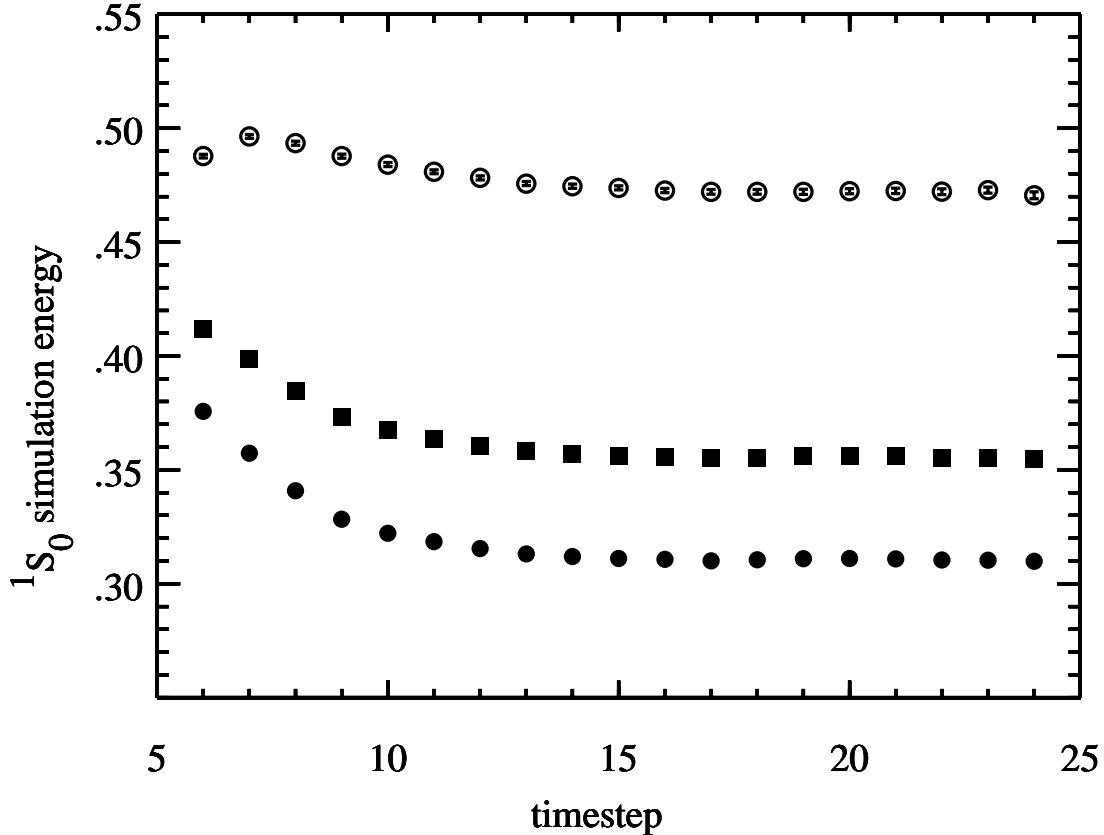


FIG. 1. Effective mass plots for the ground state heavy-light meson at rest with  $\kappa = 0.23$ , and terms up to  $O(1/(a_s M)^2)$  retained in the Hamiltonian. Only  $H_0$  is in  $H_A$  of Eq. (9). Solid circles, solid squares and open circles are for  $a_s M = 1.2, 1.5$  and  $5.0$  respectively. Statistical errors are smaller than the plotted symbols.

$L_s = N_s a_s$  is the spatial extent of the lattice in physical units. Solving for the kinetic mass gives

$$M_{\text{kin}} = \frac{2\pi^2}{N_s^2 \xi^2 a_t [a_t (E_{\mathbf{p}} - E_0)]}. \quad (34)$$

Some justification for Eq. (33) comes from consideration of the next correction term, giving

$$E_{\mathbf{p}} - E_0 = \frac{\mathbf{p}^2}{2M_{\text{kin}}} - \frac{\mathbf{p}^4}{8M_{\text{kin}}^3}. \quad (35)$$

We have verified that the extra term shifts the kinetic mass by an amount which is smaller than the uncertainties for every value of  $M_{\text{kin}}$  reported in this work.

In the case of S-wave mesons, a plateau containing ample timesteps is clearly evident in all effective mass plots; some examples are shown in Fig. 1. A more detailed discussion of the P-wave plateaus is deferred to Sec. V. In this paper, the plateau region for each mass is defined by the maximum value of

TABLE II. Examples of plateaus defined by maximization of  $Q$ . Notice that they all have the desired feature that  $Q \geq 0.1$ . Insensitivity of the fit parameters to the precise plateau boundaries has been verified.

	$^1S_0$	$^1S_0(\mathbf{p})$	$^3S_1$	$^1P_1$	$^3P_0$	$^3P_1$	$^3P_2$
$a_s M = 1.5, \kappa = 0.23$							
$(t_{\min}, t_{\max})$	(15,22)	(16,22)	(17,22)	(13,22)	(12,22)	(14,22)	(12,22)
Q	0.45	0.13	0.27	0.60	0.21	0.97	0.92
$a_s M = 1.5, \kappa = 0.24$							
$(t_{\min}, t_{\max})$	(15,20)	(16,20)	(15,20)	(12,20)	(11,20)	(14,20)	(13,20)
Q	0.22	0.14	0.61	0.69	0.26	0.86	0.43
$a_s M = 6, \kappa = 0.23$							
$(t_{\min}, t_{\max})$	(17,22)	(16,22)	(16,22)	(13,22)	(12,22)	(13,22)	(12,22)
Q	0.88	0.29	0.67	0.15	0.69	0.65	0.50
$a_s M = 6, \kappa = 0.24$							
$(t_{\min}, t_{\max})$	(16,20)	(14,20)	(16,20)	(13,20)	(12,20)	(13,20)	(12,20)
Q	0.51	0.16	0.77	0.35	0.10	0.12	0.93

$$Q \equiv \frac{\Gamma(N/2 - 1, \chi^2/2)}{\Gamma(N/2 - 1, 0)} \quad (36)$$

where

$$\Gamma(a, x) = \int_x^\infty dt t^{a-1} \exp(-t), \quad (37)$$

and  $N$  is the number of timesteps in the proposed plateau region.  $\chi^2$  is obtained from a single exponential fit to each meson correlation function. A correlated fit is done with the covariance matrix inverted by singular value decomposition. Statistical uncertainties are obtained from the analysis of 5000 bootstrap ensembles. All plateaus are ended at timestep 22(20) for simulations with  $\kappa = 0.23(0.24)$ , except for an infinitely-heavy quark due to excessive noise at these larger times. The examples in Table II demonstrate the quality of the fits.

#### IV. S-WAVE SPECTRUM

Calculations were performed for  $a_s M = 1.2, 1.5, 5, 6$  and  $\infty$ , where  $M$  represents the bare heavy quark mass in the NRQCD action. Figure 2 shows the simulation energy of the ground state as a function of  $a_s M$  for  $\kappa = 0.24$ . The huge  $O(1/M^3)$  effect at smaller  $M$  values is due to the vacuum expectation value of the  $c_{10}$  term. This large correction to the unphysical simulation energy does not discredit the convergence of NRQCD, but special care must be taken to ensure that the large vacuum value is incorporated into the heavy quark propagation appropriately. In particular, previous work [4] has shown the linear approximation to be insufficient for the  $c_{10}$  term, which contains the vacuum expectation value, in computations of the S-wave spin splitting in the charm region. Fig. 2 explicitly shows the error introduced by placing the  $c_{10}$  term in  $H_B$  rather than  $H_A$  in Eq. (9).



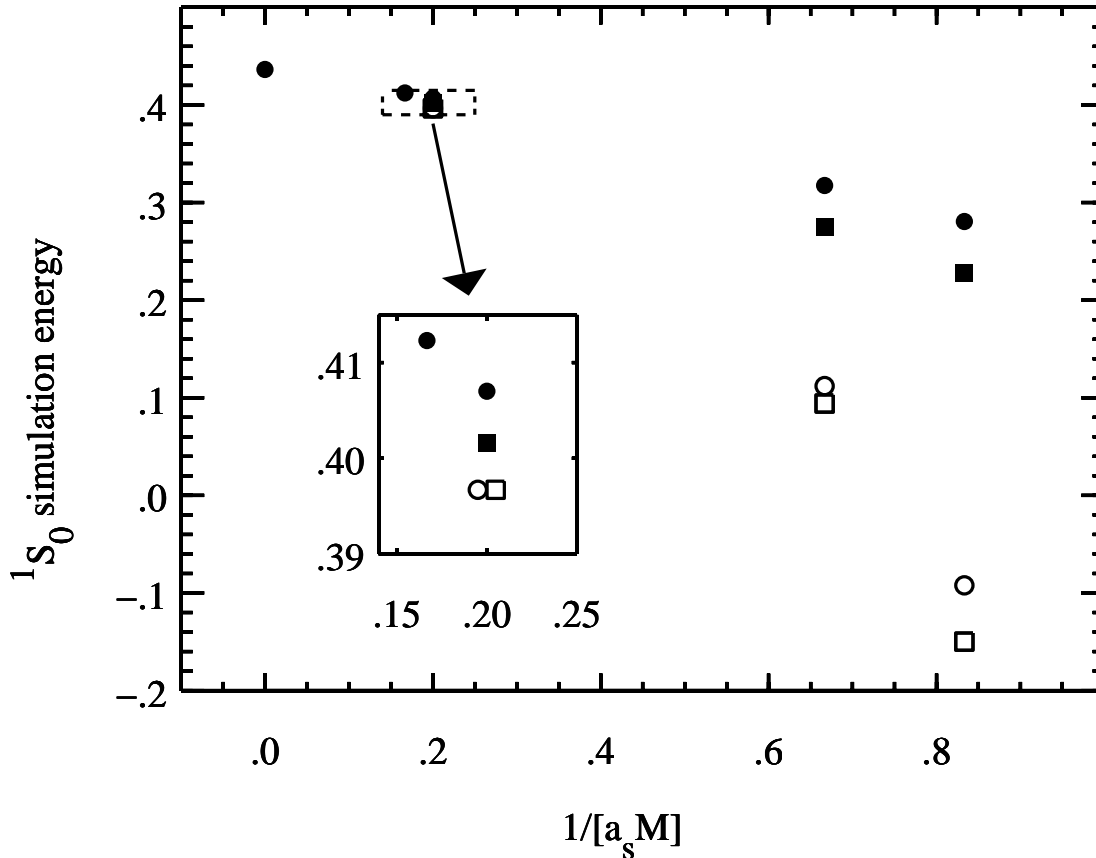


FIG. 2. The simulation energy of a ground state heavy-light meson at rest. Results are displayed from terms up to  $O(1/(a_s M)^k)$ , with  $k = 1, 2, 3$ .  $\kappa$  is fixed at 0.24, and  $M$  is the bare heavy quark mass. Solid circles are  $k = 1$ , solid squares are  $k = 2$ , open circles(squares) are  $k = 3$  with the  $c_{10}$  term in  $H_B(H_A)$  of Eq. (9). Statistical errors are smaller than the plotted symbols.

It will also be noted from Fig. 2 that the simulation energy is negative for  $a_s M = 1.2$  at third order in NRQCD. Of course the absolute energy scale is unphysical in NRQCD due to omission of the large heavy quark mass term from the leading order action, and physical quantities (i.e. mass differences) are independent of the absolute energy scale. If the simulation energy were *large* and negative, it might signal a poor  $1/M$  expansion and/or a problem for the discretization of heavy quark propagation, but a small negative result presents no problem.

Table III shows a calculation of the kinetic mass, and indicates that the bottom quark requires  $a_s M \approx 5.5$ . The charm quark seems to want  $1.2 < a_s M < 1.5$ , although the data suggest that the  $1/M$  expansion might not be converging in this region. It is interesting to notice that the vacuum expectation value does not affect the calculation of this observable significantly.

A stronger statement about convergence comes from the splitting between the spin-singlet and spin-triplet S-wave states, since the uncertainties are smaller. Table IV suggests a nice convergence in the bottom region, but no guarantee of convergence for charm. It will be noted that an incorrect treatment of the vacuum expectation value (i.e. putting the  $c_{10}$

TABLE III. The kinetic energy of a  $^1S_0$  heavy-light meson.  $H_A$  and  $H_B$  are defined by Eq. (9) and  $c_{10}$  by Eq. (15). Except for  $a_s M = 6$ , the results in physical units are computed from  $O(1/M^2)$  data, using the lattice spacing from Eq. (30) to set the physical length scale. Only statistical uncertainties are shown.

	$a_s M$	$a_t E(\vec{p}) - a_t E(\vec{0})$				$M_{\text{kin}}$ [GeV]
		$O(1/M)$	$O(1/M^2)$	$O(1/M^3)$		
				$c_{10}$ in $H_B$	$c_{10}$ in $H_A$	
$\kappa=0.23$	1.2	0.0487(10)	0.0515(10)	0.0530(10)	0.0582(39)*	1.83(6)
	1.5	0.0425(9)	0.0444(9)	0.0459(9)	0.0519(25)*	2.12(8)
	5.0	0.0185(10)	0.0188(10)	0.0188(10)	0.0239(26)*	5.0(3)
	6.0	0.0162(10)				5.8(4)
$\kappa=0.24$	1.2	0.0496(25)	0.0523(24)	0.0549(24)	0.0566(27)	1.80(10)
	1.5	0.0430(24)	0.0449(22)	0.0469(21)	0.0471(23)	2.10(12)
	5.0	0.0191(17)	0.0194(16)	0.0194(16)	0.0194(16)	4.9(4)
	6.0	0.0180(22)				5.2(7)

\*These computations use only 200 configurations.

term into  $H_B$ ) can actually lead to a small  $O(1/M^3)$  contribution, but this is incidental.

Tables III and IV correctly accommodate the vacuum expectation value of the  $c_{10}$  term by placing it in  $H_A$ . In Ref. [4], this method was found to give the same numerical results, within statistical uncertainties, for the S-wave kinetic mass and spin splitting as was obtained by computing the vacuum expectation value directly and subtracting it from the Hamiltonian. For the present calculation, a similar check was performed: the vacuum expectation value was computed from 400 of the gauge field configurations, and the S-wave kinetic mass and spin splitting were computed from 200 configurations using the Hamiltonian with the vacuum value explicitly removed. As expected, the results agree within statistics with Tables III and IV when the  $c_{10}$  term is in  $H_A$ .

Interpolating these data so that  $M_{\text{kin}}$  is the physical mass of a bottom meson, one finds a spin splitting which is only about 55% of the experimental value. This is typical of quenched lattice calculations (see for eg. Refs. [4,23,25]). Even an unquenched NRQCD calculation did not reproduce the experimental  $B^* - B$  splitting [28] so perhaps the tadpole-improved *classical* values, which were used for the coefficients  $c_i$  in the NRQCD Hamiltonian, account for the residual discrepancy.

The data reported in Ref. [4] display a  $1/M$  expansion for charmed mesons in lattice NRQCD in which  $O(1/M^3)$  terms were as significant as  $O(1/M^2)$  terms, so convergence of the expansion could not be assured. In that work, it was hoped that a more convergent expansion might be obtained via changes in the lattice method. In particular, replacement of the average plaquette tadpole factor by the mean link in Landau gauge was suggested to hold some promise. [6,7] The present work has made this modification plus a number of others including: a more aggressively-improved light quark action, asymmetric lattices with temporal spacing reduced by a factor of two, Dirichlet temporal boundaries for light quarks rather than periodic ones, smeared meson sources rather than local sources, and a symmetric dependence on  $H_B$  in Eq. (9). Despite these changes, convergence of the  $1/M$  expansion remains unconfirmed for S-wave charmed mesons. It is possible that a study of

TABLE IV. The  ${}^3S_1 - {}^1S_0$  mass splitting.  $H_A$  and  $H_B$  are defined by Eq. (9) and  $c_{10}$  by Eq. (15). Except for  $a_s M = 6$ , the results in physical units are computed from  $O(1/M^2)$  data, using the lattice spacing from Eq. (30) to set the physical length scale. Only statistical uncertainties are shown.

	$a_s M$	$a_t M({}^3S_1) - a_t M({}^1S_0)$				$M({}^3S_1) - M({}^1S_0)$ [MeV]
		$O(1/M)$	$O(1/M^2)$	$O(1/M^3)$		
				$c_{10}$ in $H_B$	$c_{10}$ in $H_A$	
$\kappa=0.23$	1.2	0.0441(6)	0.0527(7)	0.0508(7)	0.0566(25)*	96.6(24)
	1.5	0.0385(6)	0.0447(6)	0.0447(6)	0.0452(19)*	81.9(21)
	5.0	0.0155(4)	0.0165(4)	0.0165(4)	0.0159(8)*	30.2(10)
	6.0	0.0136(5)				24.9(11)
$\kappa=0.24$	1.2	0.0483(11)	0.0589(12)	0.0577(11)	0.0677(15)	107.9(32)
	1.5	0.0418(9)	0.0494(11)	0.0502(10)	0.0554(11)	90.5(28)
	5.0	0.0147(13)	0.0157(13)	0.0158(13)	0.0158(13)	28.8(25)
	6.0	0.0136(7)				24.9(14)

\*These computations use only 200 configurations.

terms beyond  $O(1/M^3)$  would reveal that the series really is well-behaved, but this remains unexplored.

## V. P-WAVE SPECTRUM

Each of the four P-wave operators from Table I leads to a visually-identifiable plateau; an example is shown in Fig. 3. The method of maximum  $Q$ , discussed in Sec. III, can be used to define precise plateau boundaries and the resultant  ${}^3P_0 - {}^1S_0$  splitting is shown in Table V. In contrast to the S-wave splitting discussed in the previous section, the  $1/M$  corrections to the  ${}^3P_0 - {}^1S_0$  splitting are not large relative to the statistical uncertainties, even in the charm region. The splittings given in Table V are consistent with the available experimental data, as will be discussed below.

Tables VI and VII contain lattice results for splittings which involve the other P-wave mesons. In the charm region, the  $\kappa = 0.23$  data produce a  ${}^3P_2$  meson which is heavier than the  ${}^3P_0$  meson, but at  $\kappa = 0.24$  the  ${}^3P_2 - {}^3P_0$  splitting is consistent with zero. The magnitudes of the splittings decrease in the bottom region, as expected.

A comparison of Tables V, VI and VII plus the effective mass plots in Fig. 4 provide some indication of the systematic uncertainty which arises from the choice of plateau region. In particular, it will be noted that the effective mass plots are monotonically decreasing near the source, so if a plateau region is chosen too near the source, it will produce a mass splitting which is too large. Thus one arrives at an upper bound for the  ${}^3P_2 - {}^3P_0$  splitting, as presented in Ref. [24].

The correlation functions constructed using  ${}^1P_1$  and  ${}^3P_1$  operators contain some combination of the physical  $J = 1$  mesons. Both calculations should lead to the same (lighter) physical mass at large Euclidean times if both operators have a substantial overlap with the less massive  $J = 1$  state. In principle, the masses of the physical states can be obtained

TABLE V. The  ${}^3P_0 - {}^1S_0$  mass splitting.  $H_A$  and  $H_B$  are defined by Eq. (9) and  $c_{10}$  by Eq. (15). Except for  $a_s M = 6$  and  $a_s M = \infty$ , the results in physical units are computed from  $O(1/M^2)$  data, using the lattice spacing from Eq. (30) to set the physical length scale. Only statistical uncertainties are shown.

	$a_s M$	$a_t M({}^3P_0) - a_t M({}^1S_0)$				$M({}^3P_0) - M({}^1S_0)$ [MeV]
		$O(1/M)$	$O(1/M^2)$	$O(1/M^3)$		
				$c_{10}$ in $H_B$	$c_{10}$ in $H_A$	
$\kappa=0.23$	1.2	0.275(5)	0.271(4)	0.276(4)	0.277(16)*	497(13)
	1.5	0.266(5)	0.263(4)	0.267(4)	0.268(10)*	482(13)
	5.0	0.238(5)	0.238(4)	0.238(4)	0.252(11)*	436(12)
	6.0	0.236(5)				432(13)
	$\infty$	0.225(5)				412(13)
$\kappa=0.24$	1.2	0.311(6)	0.311(6)	0.315(6)	0.321(7)	570(16)
	1.5	0.300(6)	0.301(6)	0.304(6)	0.306(6)	552(16)
	5.0	0.256(8)	0.256(7)	0.256(7)	0.256(7)	469(16)
	6.0	0.254(8)				465(18)
	$\infty$	0.210(20)				385(38)

\*These computations use only 200 configurations.

TABLE VI. The  ${}^1P_1 - {}^1S_0$ ,  ${}^3P_1 - {}^1S_0$  and  ${}^3P_2 - {}^1S_0$  mass splittings. Data at  $a_s M = 6$  use the Hamiltonian up to  $O(1/M)$  and data at  $a_s M < 6$  use the Hamiltonian up to  $O(1/M^2)$ . Only statistical uncertainties are shown.

	$a_s M$	$a_t M(X) - a_t M({}^1S_0)$		
		$X = {}^1P_1$	$X = {}^3P_1$	$X = {}^3P_2$
$\kappa=0.23$	1.2	0.288(7)	0.298(9)	0.325(7)
	1.5	0.279(7)	0.285(8)	0.311(7)
	5.0	0.236(8)	0.246(7)	0.259(7)
	6.0	0.240(7)	0.243(8)	0.253(7)
	$\infty$	0.181(26)	0.226(10)	0.214(11)
$\kappa=0.24$	1.2	0.295(13)	0.309(20)	0.327(18)
	1.5	0.295(10)	0.294(19)	0.315(17)
	5.0	0.232(15)	0.250(14)	0.270(13)
	6.0	0.225(16)	0.246(15)	0.265(13)
	$\infty$	0.200(32)	0.257(61)	0.219(17)

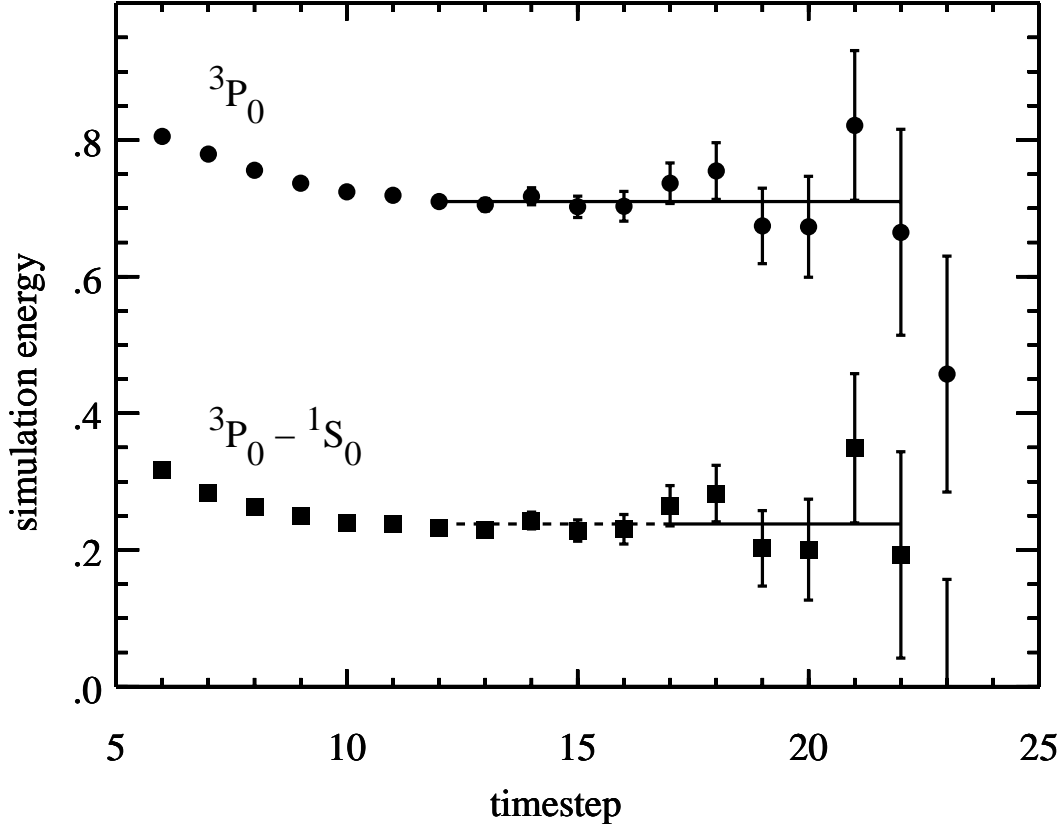


FIG. 3. The simulation energy of a  ${}^3P_0$  heavy-light meson, for  $\kappa = 0.23$  and  $a_s M = 5.0$ . The Hamiltonian contains all terms up to and including  $O(1/(a_s M)^2)$ . The splitting between the  ${}^3P_0$  and  ${}^1S_0$  is also shown.

using the  ${}^1P_1/{}^3P_1$  operator basis by also calculating the mixing matrix elements, but the effect was too small to be observed in these data. In practice, for Euclidean times which can be used in our lattice simulation, no significant energy difference is observed between the  ${}^1P_1$  and  ${}^3P_1$  channels.

Predictions for the physical mesons are displayed alongside experimental data in Table VIII. The  $D_s - D$  and  $B_s - B$  mass differences depend only mildly on  $O(1/M^2)$  and  $O(1/M^3)$  terms, and they are close to experiment. In contrast, the S-wave spin splittings are significantly smaller than experiment (as is typical of quenched lattice QCD [4,23,25]). Furthermore, the  $O(1/M^2)$  and  $O(1/M^3)$  corrections to  $D^* - D$  are each about 20% of the leading order result. The results in Table VIII use the value of  $\kappa_s$  determined from  $m_K$  in Eq. (29). Use of the other determination in Eq. (29) shifts the central values of the  $D_s^* - D_s$  and  $B_s^* - B_s$  mass splittings by 1 MeV or less, and shifts the splittings among P-waves ( $D_s^{**}$  and  $B_s^{**}$ ) by 7 MeV or less.

A detailed comparison of P-wave results would be somewhat premature, since the experimental data are rather incomplete and often rely on theoretical models for input, while the lattice calculation is quenched and lacks a firm connection between the physical mesons and the  $J = 1$  operators. Nevertheless, Table VIII shows a general consistency between the

TABLE VII. The  $^1P_1 - ^3P_0$ ,  $^3P_1 - ^3P_0$  and  $^3P_2 - ^3P_0$  mass splittings. Data at  $a_s M = 6$  use the Hamiltonian up to  $O(1/M)$  and data at  $a_s M < 6$  use the Hamiltonian up to  $O(1/M^2)$ . Only statistical uncertainties are shown.

	$a_s M$	$a_t M(X) - a_t M(^3P_0)$		
		$X = ^1P_1$	$X = ^3P_1$	$X = ^3P_2$
$\kappa=0.23$	1.2	0.017(7)	0.027(9)	0.054(7)
	1.5	0.015(7)	0.021(8)	0.047(7)
	5.0	-0.002(8)	0.008(6)	0.021(7)
	6.0	0.004(7)	0.007(7)	0.017(7)
	$\infty$	-0.044(26)	0.001(9)	-0.011(11)
$\kappa=0.24$	1.2	-0.016(14)	-0.002(20)	0.016(19)
	1.5	-0.005(10)	-0.007(19)	0.014(17)
	5.0	-0.024(16)	-0.006(13)	0.014(14)
	6.0	-0.029(17)	-0.008(14)	0.011(15)
	$\infty$	-0.010(32)	0.047(21)	0.009(27)

experimental and computed P-wave masses.

It is instructive to compare lattice P-wave masses to the predictions of models, such as quark models [14,20,21], a Bethe-Salpeter study [15], a chromodynamic potential model [16], a bag model [17] and a Blankenbecler-Sugar approach [18]. Many of these present results for  $J = 1$  directly in the  $^1P_1/^3P_1$  basis which simplifies the comparison to lattice data, and the quark models may in general be more closely related to the quenched approximation than to experiment.

The models of Refs. [14–16,18] predict the traditional hydrogen-like ordering of P-waves, where the  $^3P_0$  is the lightest meson, the  $^3P_2$  is the heaviest, and the  $P_1$  states lie in between. The authors of Ref. [17] find, from lightest to heaviest,  $^3P_0$ ,  $P_1(3/2)$ ,  $^3P_2$ ,  $P_1(1/2)$ , where the arguments represent the angular momentum of the light degrees of freedom. Ref. [20] predicts a dramatic inversion where the  $^3P_0$  is heavier than the  $^3P_2$  by 100(150) MeV for  $D^{**}(B^{**})$  mesons, but the  $P_1$  states are the absolute lightest and heaviest. Ref. [21] claims very small splittings (tens of MeV) where the  $P(1/2)$  and  $P(3/2)$  doublets overlap to produce different orderings for the  $D$ ,  $D_s$  and  $B$  systems (the  $B_s$  is ordered like the  $D$ ).

Fig. 5 shows the  $D_2^* - D_0^*$  and  $B_2^* - B_0^*$  splittings from lattice QCD and from the models just mentioned. Despite the range of model predictions, it is evident that some general consistency exists between our results and a number of the models. Notice in particular that our results are numerically distinct from the large inversion of Ref. [20]. Fig. 6 compares the  $^3P_0 - ^1S_0$  splittings as obtained from lattice QCD and the models.

Of special importance is the comparison with Ref. [25], where the spectrum was also computed from quenched lattice NRQCD. The discrepancy between the two lattice calculations is exemplified by Fig. 5. While there are many differences in method between the two computations, it is difficult to identify a compelling reason for the disagreement. Fig. 4 indicates that our data must satisfy  $M(B_2^*) - M(B_0^*) < 100$  MeV for any chosen plateau region, and this is not consistent with Ref. [25]. It is hoped that further lattice efforts will improve this situation. Unfortunately, a recent lattice NRQCD study of the heavy-light me-

TABLE VIII. The heavy-light spectrum compared to experiment. The hadron naming scheme of Ref. [29] is followed [30]. The charm and bottom masses are fixed to the experimental  $D_s$  and  $B_s$  masses (giving  $a_s M_c = 1.37(8)$  and  $a_s M_b = 5.8({}_{-6}^{+13})$ ). The first uncertainty on lattice data combines the statistical error with the uncertainty of  $a_t$  from Eq. (30). The second uncertainty on lattice data corresponds to the errors in  $a_s M_c$  and  $a_s M_b$ . The value of  $\kappa_s$  determined from  $m_K$  in Eq. (29) has been used.

charmed meson masses [MeV]			bottom meson masses [MeV]		
	experiment/Ref.	lattice		experiment/Ref.	lattice
$D_s$	1969(1)/ [29]	input	$B_s$	5369(2)/ [29]	input
$D_s^* - D_s$	144/ [29]	$O(1/M):79(2)(3)$ $O(1/M^2):94(2)(5)$ $O(1/M^3):103(3)(6)$	$B_s^* - B_s$	47(3)/ [29]	26(1)( ${}_{-6}^{+3}$ )
$D_{s0}^* - D_s$		530(13)(5)	$B_{s0}^* - B_s$		451(15)( ${}_{-6}^{+3}$ )
$D'_{s1} - D_s$		${}^1P_1:531(16)(2)$	$B'_{s1} - B_s$		${}^1P_1:425(24)({}_{-5}^{+2})$
$D_{s1} - D_s$	566(1)/ [29]	${}^3P_1:542(22)(8)$	$B_{s1} - B_s$		${}^3P_1:449(22)({}_{-9}^{+5})$
$D_{s2}^* - D_s$	604(2)/ [29]	585(19)(6)	$B_{s2}^* - B_s$		478(21)( ${}_{-12}^{+6}$ )
			$(B_s^{**} - B_s)$	484(15)/ [29]†	
$D_s - D$	99,104/ [29]	$O(1/M):105(2)(1)$ $O(1/M^2):107(3)(1)$ $O(1/M^3):112(4)(1)$	$B_s - B$	90(2)/ [29]	92(3)( ${}_{-0}^{+1}$ )
$D^* - D$	141,142/ [29]	$O(1/M):84(3)(3)$ $O(1/M^2):101(3)(5)$ $O(1/M^3):117(4)(6)$	$B^* - B$	46/ [29]	25(2)( ${}_{-4}^{+3}$ )
$D_0^* - D$		579(15)(5)	$B_0^* - B$		475(19)( ${}_{-6}^{+4}$ )
$D'_1 - D$	596(53)/ [10]	${}^1P_1:548(20)(2)$	$B'_1 - B$	391(16)/ [12]*	${}^1P_1:407(38)({}_{-24}^{+11})$
$D_1 - D$	558(2)/ [10]	${}^3P_1:557(32)(8)$	$B_1 - B$	431(20)/ [11]*	${}^3P_1:453(33)({}_{-10}^{+5})$
$D_2^* - D$	595(2)/ [29]	588(30)(6)	$B_2^* - B$	489(8)/ [12]* 460(13)/ [13]*	493(29)( ${}_{-13}^{+5}$ )
			$(B^{**} - B)$	418(9)/ [29]†	

†Experimental signal is a sum over resonances with differing momenta  $J = 0, 1, 2$ .

\*Theoretical estimates for some of the mass splittings have been used as input.

son spectrum [26] has statistical uncertainties which are too large to resolve the discrepancy between our results and those of Ref. [25].

## VI. CONCLUSIONS

The masses of S and P-wave heavy-light mesons have been calculated in the quenched approximation, using lattice NRQCD for the heavy quark and a highly-improved action for the light degrees of freedom. Calculations at first, second and third order in the heavy quark mass expansion were used as a test of convergence, and it was concluded that the  $O(1/M^2)$  and  $O(1/M^3)$  contributions to the  $D^* - D$  splitting are both near 20%. The  $D_s^* - D_s$  splitting receives a 20% correction at  $O(1/M^2)$  and a 10% correction at  $O(1/M^3)$ . These results might represent a convergent  $1/M$  expansion if terms beyond  $O(1/M^3)$  are decreasing appropriately, but convergence cannot be ascertained from the present study. This same conclusion was reached in Ref. [4] by a computational method which differed from the present one in some details; most notably, Ref. [4] used the average plaquette tadpole definition whereas the present work uses the mean link in Landau gauge.

No convergence problem is found for P-wave charmed masses, and the P-wave spectrum for both charmed and bottom mesons is predicted. The  ${}^3P_2$  is heavier than the  ${}^3P_0$  and  $P_1$  states in the  $D_s^{**}$  system, with  $M(D_{s2}^*) - M(D_{s0}^*) = 55 \pm 17$  MeV. For the  $D^{**}$ ,  $B^{**}$  and  $B_s^{**}$  systems the  $P_2 - P_0$  splittings are smaller and consistent with zero. These conclusions agree with a number of model calculations and are compatible with the available experimental data.

## ACKNOWLEDGMENTS

The authors thank Howard Trottier for a critical reading of the manuscript, and R.L. thanks Niranjana Venugopal for useful discussions. This work was supported in part by the Natural Sciences and Engineering Research Council of Canada.



## REFERENCES

- [1] N. Isgur and M. B. Wise, Phys. Lett. B **232**, 113 (1989); Phys. Lett. B **237**, 527 (1990).
- [2] W. E. Caswell and G. P. Lepage, Phys. Lett. B **167**, 437 (1986); G. P. Lepage and B. A. Thacker, Nucl. Phys. B (Proc. Suppl.) **4**, 199 (1988); B. A. Thacker and G. P. Lepage, Phys. Rev. D **43**, 196 (1991); G. T. Bodwin, E. Braaten and G. P. Lepage, Phys. Rev. D **51**, 1125 (1995).
- [3] G. P. Lepage, L. Magnea, C. Nakhleh, U. Magnea and K. Hornbostel, Phys. Rev. D **46**, 4052 (1992).
- [4] R. Lewis and R. M. Woloshyn, Phys. Rev. D **58**, 074506 (1998); R. Lewis and R. M. Woloshyn, Nucl. Phys. B (Proc. Suppl.) **73**, 333 (1999).
- [5] For a review, see A. Ali Khan, Nucl. Phys. B (Proc. Suppl.) **63**, 71 (1998).
- [6] P. Lepage, Nucl. Phys. A (Proc. Suppl.) **60**, 267 (1998); M. Alford, T. R. Klassen and P. Lepage, Nucl. Phys. B (Proc. Suppl.) **63**, 862 (1998).
- [7] H. D. Trottier, Phys. Rev. D **55**, 6844 (1997); N. H. Shakespeare and H. D. Trottier, Phys. Rev. D **58**, 034502 (1998).
- [8] M. Alford, T. R. Klassen and G. P. Lepage, Nucl. Phys. B **496**, 377 (1997).
- [9] For a recent review, see V. Ciulli, hep-ex/9911044 to be published in proceedings of Heavy Flavours 8, Southampton, UK, 1999.
- [10] J. L. Rodriquez (CLEO Collaboration), hep-ex/9901008 (1999); S. Anderson *et al.* (CLEO Collaboration), Nucl. Phys. A **663**, 647 (2000).
- [11] G. Bauer (CDF Collaboration), hep-ex/9909014 (1999).
- [12] M. Acciari *et al.* (L3 Collaboration), Phys. Lett. B **465**, 323 (1999).
- [13] R. Barate *et al.* (ALEPH Collaboration), Phys. Lett. B **425**, 215 (1998).
- [14] S. Godfrey and R. Kokoski, Phys. Rev. D **43**, 1679 (1991).
- [15] Y. Dai, C. Huang and H. Jin, Phys. Lett. B **331**, 174 (1994).
- [16] S. N. Gupta and J. M. Johnson, Phys. Rev. D **51**, 168 (1995).
- [17] A. H. Orsland and H. Hogaasen, Eur. Phys. J. C **9**, 503 (1999).
- [18] T. A. Lähde, C. J. Nyfält and D. O. Riska, Nucl. Phys. A **674**, 141 (2000).
- [19] H. J. Schnitzer, Phys. Lett. B **76**, 461 (1978); Nucl. Phys. B **207**, 131 (1982).
- [20] N. Isgur, Phys. Rev. D **57**, 4041 (1998).
- [21] D. Ebert, V. O. Galkin and R. N. Faustov, Phys. Rev. D **57**, 5663 (1998); erratum *ibid.* **59**, 019902 (1999).
- [22] C. Michael and J. Peisa, Phys. Rev. D **58**, 034506 (1998).
- [23] P. Boyle, Nucl. Phys. B (Proc. Suppl.) **63**, 314 (1998).
- [24] R. Lewis and R. M. Woloshyn, Nucl. Phys. B (Proc. Suppl.) **83-84**, 316 (2000).
- [25] A. Ali Khan *et al.* hep-lat/9912034 (1999).
- [26] J. Hein *et al.* hep-ph/0003130 (2000).
- [27] A. V. Manohar, Phys. Rev. D **56**, 230 (1997); C. Balzereit, Phys. Rev. D **59**, 034006 (1999).
- [28] S. Collins *et al.*, Phys. Rev. D **60**, 074504 (1999).
- [29] C. Caso *et al.*, The European Physical Journal C3 (1998) 1 and 1999 off-year partial update for the 2000 edition available on the PDG WWW pages (URL: <http://pdg.lbl.gov/>).
- [30] A ' is used to distinguish between the two physical  $J = 1$  states. The ' superscript will

be used for the state which in the heavy quark spin symmetry classification has light degrees of freedom with angular momentum of  $j_l = 1/2$  and which is expected to have a large width. The unprimed  $J = 1$  state corresponds to  $j_l = 3/2$  and is expected to be narrow.

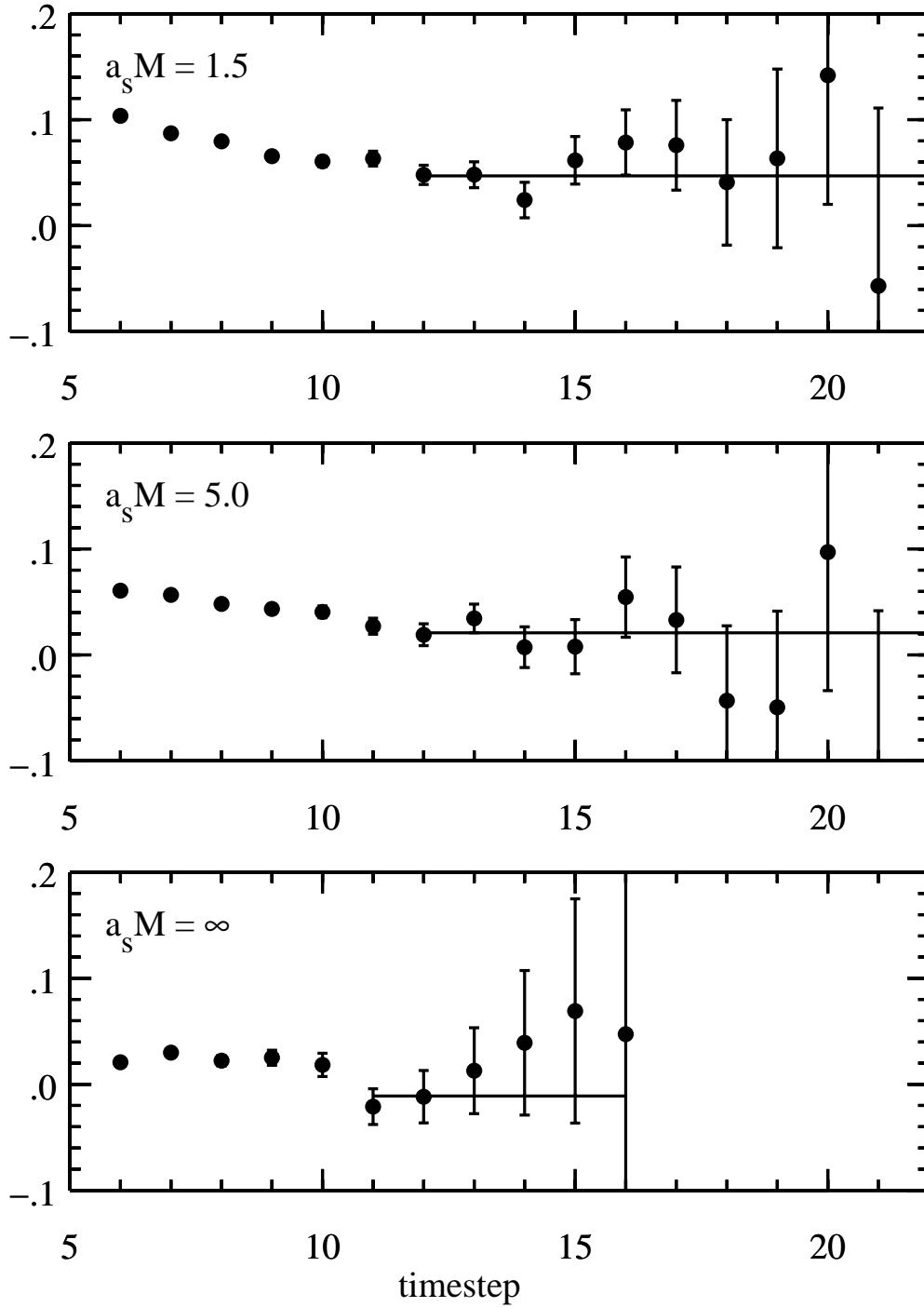
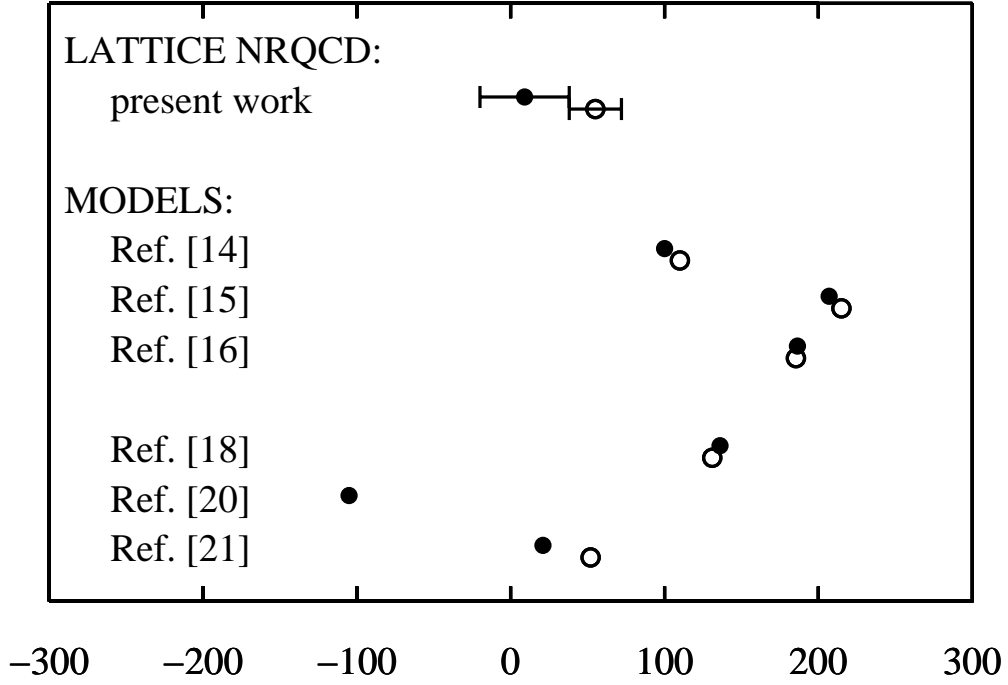


FIG. 4. Effective mass plots for the  ${}^3P_2 - {}^3P_0$  mass splitting with  $\kappa = 0.23$  and  $a_s M = 1.5, 5.0$  and  $\infty$ . The plateau region and value is also shown.

(a)  $D_2^* - D_0^*$  and  $D_{s2}^* - D_{s0}^*$



(b)  $B_2^* - B_0^*$  and  $B_{s2}^* - B_{s0}^*$

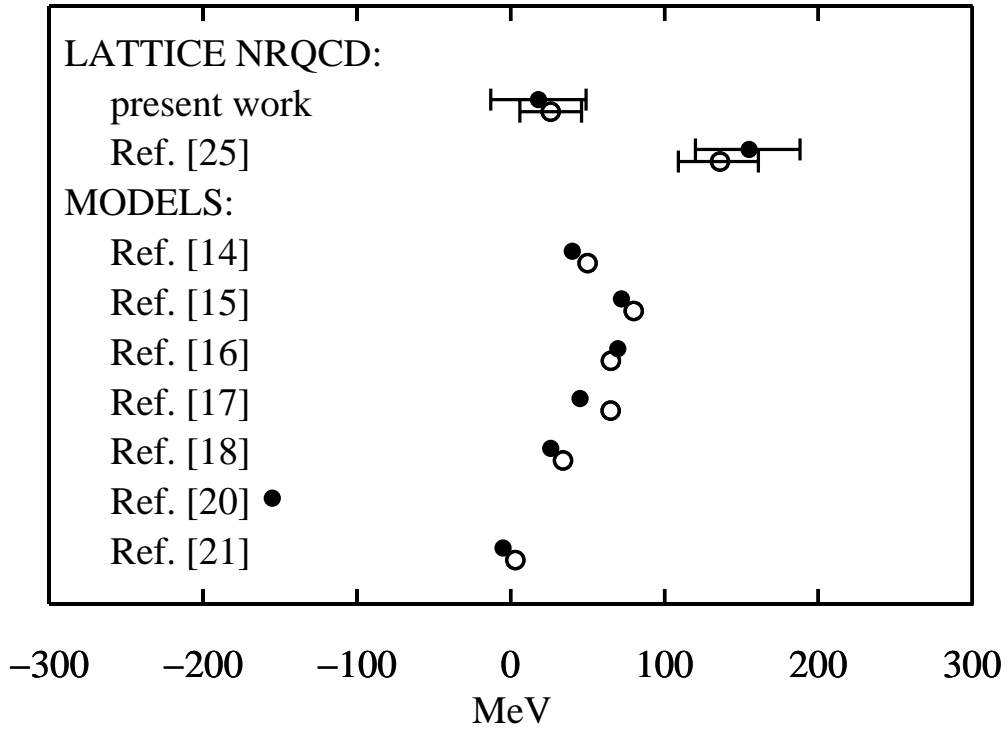
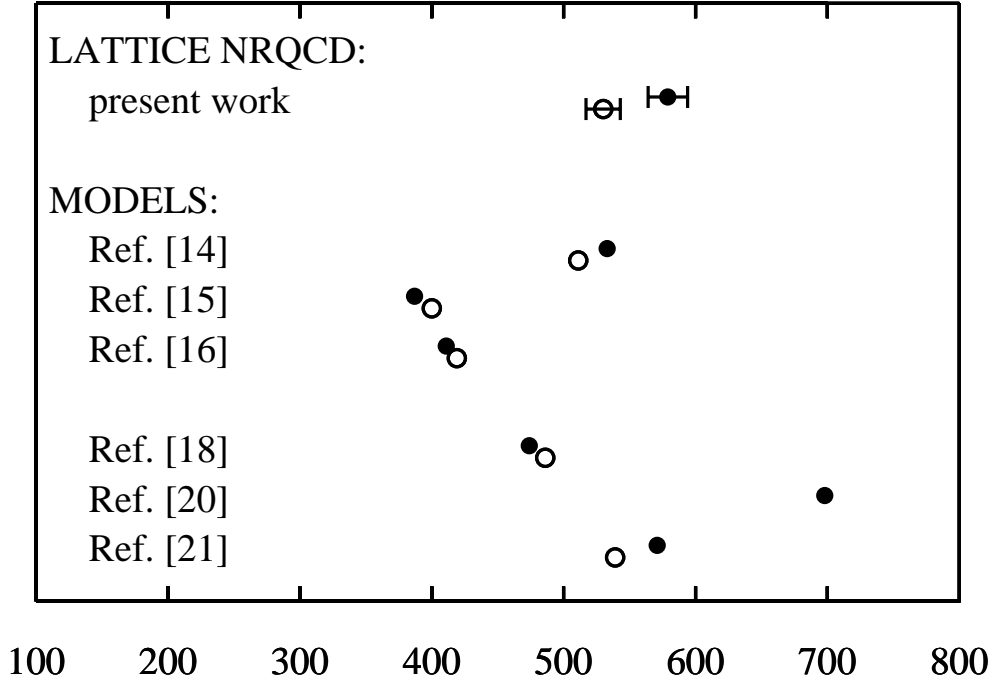


FIG. 5. The  $D_2^* - D_0^*$  and  $B_2^* - B_0^*$  splittings (solid symbols) and the  $D_{s2}^* - D_{s0}^*$  and  $B_{s2}^* - B_{s0}^*$  splittings (open symbols) from lattice QCD and various model calculations.

(a)  $D_0^* - D$  and  $D_{s0}^* - D_s$



(b)  $B_0^* - B$  and  $B_{s0}^* - B_s$

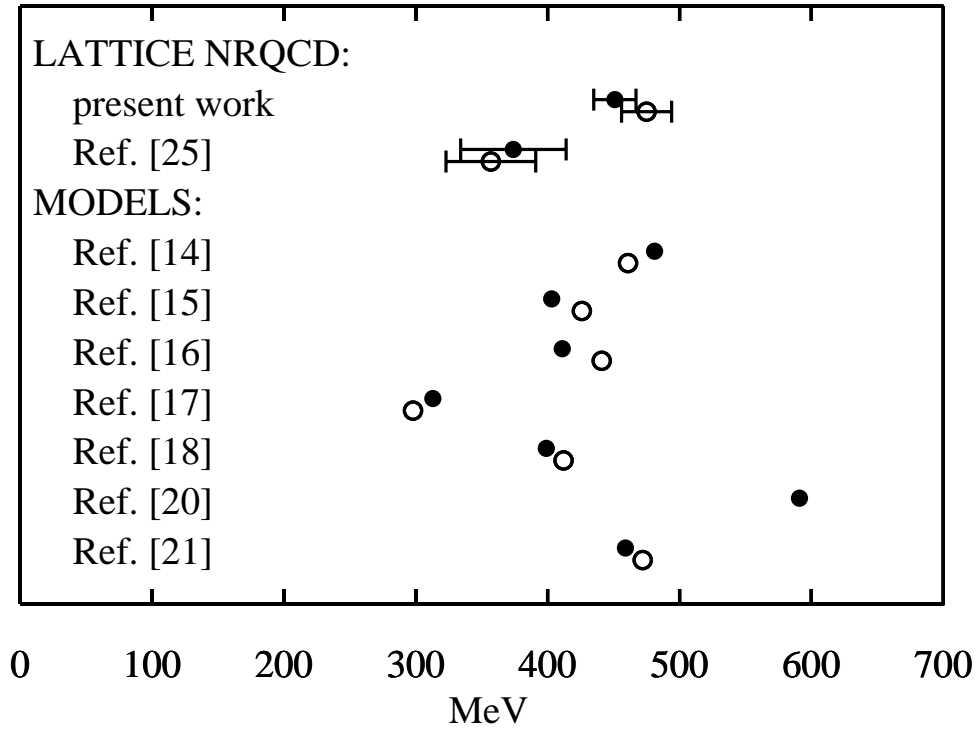


FIG. 6. The  $D_0^* - D$  and  $B_0^* - B$  splittings (solid symbols) and the  $D_{s0}^* - D_s$  and  $B_{s0}^* - B_s$  splittings (open symbols) from lattice QCD and various model calculations.